Supporting Information

Lee et al. 10.1073/pnas.1002849107

SI Text

Generalized Multiparticle Mie Theory. We use the rigorous Generalized Mie Theory (GMT) approach (also called the rigorous theory of multipole expansions) (1–5) to provide a support and interpretation of our experimental data. Although the application domain of GMT is restricted to spherical scatterers, it yields the analytical solution of the scattering problem and results in highly efficient algorithms. In the frame of GMT approach, the electromagnetic field in a photonic structure of L nanoparticles can be constructed as a superposition of partial fields scattered from each particle. These partial scattered fields as well as the incident field and internal fields are expanded in the orthogonal basis of vector spherical harmonics represented in local coordinate systems associated with individual particles:

$$\mathbf{E}^l_{\mathrm{sc}} = \sum_{n=1}^{\infty} \sum_{m=-n}^{n} (a^l_{mn}\mathbf{N}_{mn} + b^l_{mn}\mathbf{M}_{mn}), \qquad l = 1,\ldots L. \qquad \textbf{[S1]}$$

The use of the powerful addition (translation) theorem for vector spherical harmonics enables the transformation (translation) of the series expansion for the partial fields of the l-th particle into an expansion in the local coordinate system associated with any other particle of the array. A general matrix equation for the Lorenz-Mie multipole scattering coefficients (a^l_{mn}, b^l_{mn}) can be obtained by imposing the electromagnetic boundary conditions for the tangential components of the electric and magnetic fields and by truncating the infinite series expansions to a maximum multipolar order N:

$$a^l_{mn} + \tilde{a}^l_n \sum_{j\neq l}^{(1,L)} \sum_{\nu=1}^{N} \sum_{\mu=-\nu}^{\nu} (A^{jl}_{mn\mu\nu} a^j_{\mu\nu} + B^{jl}_{mn\mu\nu} b^j_{\mu\nu}) = \tilde{a}^l_n p^l_{mn}$$

$$b^l_{mn} + \tilde{b}^l_n \sum_{j\neq l}^{(1,L)} \sum_{\nu=1}^{N} \sum_{\mu=-\nu}^{\nu} (B^{jl}_{mn\mu\nu} a^j_{\mu\nu} + A^{jl}_{mn\mu\nu} b^j_{\mu\nu}) = \tilde{b}^l_n q^l_{mn}. \qquad \textbf{[S2]}$$

Here, $A^{jl}_{mn\mu\nu}$, $B^{jl}_{mn\mu\nu}$ are the translation matrices, which only depend on the distance and direction of translation from origin l to origin j (1–4), $\tilde{a}^l_n$, $\tilde{b}^l_n$ are the Mie scattering coefficients of l-th sphere in the free space (5); and p^l_{mn}, q^l_{mn} are the expansion coefficients of the incident field. Once truncated matrix Eq. **S2** are solved for the scattering coefficients, the scattering, extinction, and absorption cross-sections as well as the scattered field distributions can be accurately calculated at any desired level of accuracy. The numerical solution of Eq. **S2** can be obtained with a machine precision if the matrix equation is truncated at a high enough multipolar order.

Image Correlation Analysis of Colorimetric Fingerprint. We define the autocorrelation function (ACF) $G(\xi)$ of a fluctuating spatial signal $s(x)$ that describes the colorimetric fingerprint of nanoparticle arrays as:

$$G(\xi) = \langle s(x)s(x+\xi)\rangle, \qquad \textbf{[S3]}$$

where the angle brackets $\langle\rangle$, indicate averaging (integration) over the spatial domain. In order to properly extract quantitative information, the spatial signal needs to be correctly normalized by defining the following quantity (6):

$$\delta s(x) = \frac{s(x) - \langle s(x)\rangle}{\langle s(x)\rangle} \qquad \textbf{[S4]}$$

which enables proper definition of the normalized ACF:

$$g(\xi) = \langle \delta s(x)\delta s(x+\xi)\rangle = \frac{\langle s(x)s(x+\xi)\rangle - \langle s(x)\rangle^2}{\langle s(x)\rangle^2} = \frac{G(\xi)}{\langle s(x)\rangle^2} - 1. \qquad \textbf{[S5]}$$

Analogously, for a colorimetric fingerprint in two spatial dimensions, $s(x,y)$, we can define the two-dimensional normalized ACF as:

$$g(\xi,\eta) = \langle \delta s(x,y)\delta s(x+\xi,y+\eta)\rangle = \frac{G(\xi,\eta)}{\langle s(x,y)\rangle^2} - 1. \qquad \textbf{[S6]}$$

If the colorimetric fingerprint consists of an image with $N \times M$ pixels, the discrete implementation of the spatially averaged ACF is readily obtained as:

$$g(\xi,\eta) = \frac{(1/NM)\sum_{k=1}^{N}\sum_{l=1}^{M} s(k,l)s(k+\xi,l+\eta)}{[(1/NM)\sum_{k=1}^{N}\sum_{l=1}^{M} s(k,l)]^2} - 1. \qquad \textbf{[S7]}$$

We notice that this definition of normalized ACF enables us to obtain the variance of the spatial fluctuations of the colorimetric fingerprints by simple evaluation of the autocorrelation function in the limit when both ξ and η vanish (6):

$$\mathrm{var}\,\delta s(x,y) = \lim_{\xi\to 0}\lim_{\eta\to 0} g(\xi,\eta) = g(0,0). \qquad \textbf{[S8]}$$

In this paper, in order to perform the ACF calculations more efficiently, we have resorted to the well known Fourier transform relation (6, 7):

$$G(\xi,\eta) = F^{-1}\{[F(s(x,y))] * [F^*(s(x,y))]\}. \qquad \textbf{[S9]}$$

Once $G(\xi,\eta)$ has been readily obtained from Eq. **S9**, we calculated the normalized ACF directly by using Eq. **S6**. The normalized ACF profiles in one spatial dimension (see Fig. 5 of the paper) are extracted from the two-dimensional normalized ACF along the center line (x axis) of the image and have been normalized with respect to the size of the array along the x-direction of the image.

General Principles of Linear Response Theory. Our findings demonstrate that the colorimetric fingerprints of aperiodic structures with continuous spatial Fourier spectra are the most sensitive to small perturbation of the refractive index. This fact, which we have proved using full vector analytical Mie theory, can be more generally understood based on the general principles of linear response theory for stationary random signals. This theory provides the most general rationale to understand the scattering properties by rough surfaces in the linear optics regime. (We notice that the stationary hypothesis on the spatial signal (the scattering surface) is well satisfied in the limit of large samples). In fact, as long as the system's response is linear, we can express the mean square value of the system's output function $E[y^2]$ (which in rough surface scattering corresponds to the scattered mean field fluctuations) as follows (8):

$$E[y^2] = \int_{-\infty}^{+\infty} |H(\omega)|^2 S_x(\omega) d\omega, \qquad \textbf{[S10]}$$

where $H(\omega)$ is the linear optical transfer function of the system (frequency response), $S_x(\omega)$ is the spectral density of the nanostructured surface (defined by the Fourier transform of its autocorrelation function), and ω is a two-dimensional vector of spatial frequencies. It is evident from Eq. **S10** that the spectral character, in particular the flatness of the spectral density, of aperiodic arrays directly determines the intensity of the scattered field fluctuations. These fluctuations will be stronger for aperiodic arrays with "diffused" or flat Fourier spectra such as Rudin-Shapiro and Gaussian prime lattices. Therefore, Fourier space engineering of aperiodic arrays provides a simple tool for the optimization of the scattering response of deterministic aperiodic surfaces and allows to select the most appropriate surface structures to match specific application needs.

1. Mackowski DW (1994) Calculation of total cross sections of multiple-sphere clusters. *J Opt Soc Am A* 11:2851–2861.
2. Quinten M, Kreibig U (1993) Absorption and elastic-scattering of light by particle aggregates. *Appl Opt* 32:6173–6182.
3. Xu Y (1995) Electromagnetic scattering by an aggregate of spheres. *Appl Opt* 34:4573–4588.
4. Kreibig U, Vollme M (1995) *Optical properties of metal clusters.* (Springer-Verlag, Berlin).
5. Bohren CF, Huffman DR (1998) *Absorption and scattering of light by small particles.* (John-Wiley and Sons, New York).
6. Wiseman PW, Petersen NO (1999) Image correlation spectroscopy. II. optimization for ultrasensitive detection of preexisting platelet-derived growth factor-beta receptor oligomers on intact cells. *Biophys J* 76:963–977.
7. Petersen NO, Höddelius PL, Wiseman PW, Seger O, Magnusson KE (1993) Quantification of membrane receptor distributions by image correlation spectroscopy: concept and application. *Biophys J* 65:1135–1146.
8. Newland DE (2005) *An introduction to random vibrations, spectral and wavelet analysis*, 3rd edition, (Dover Publications, New York)

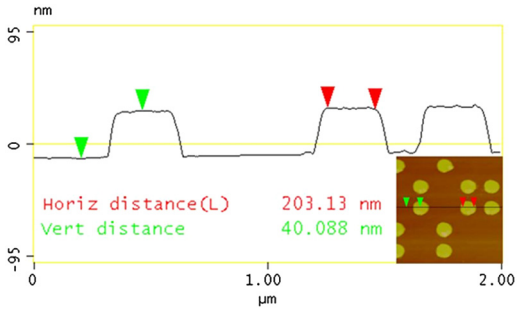

Fig. S1. Atomic force microscopy (AFM) image of a Thue-Morse array with 40 nm-high, 100 nm-radius Cr nanoparticles, and minimum center-to-center interparticle separation of 400 nm.

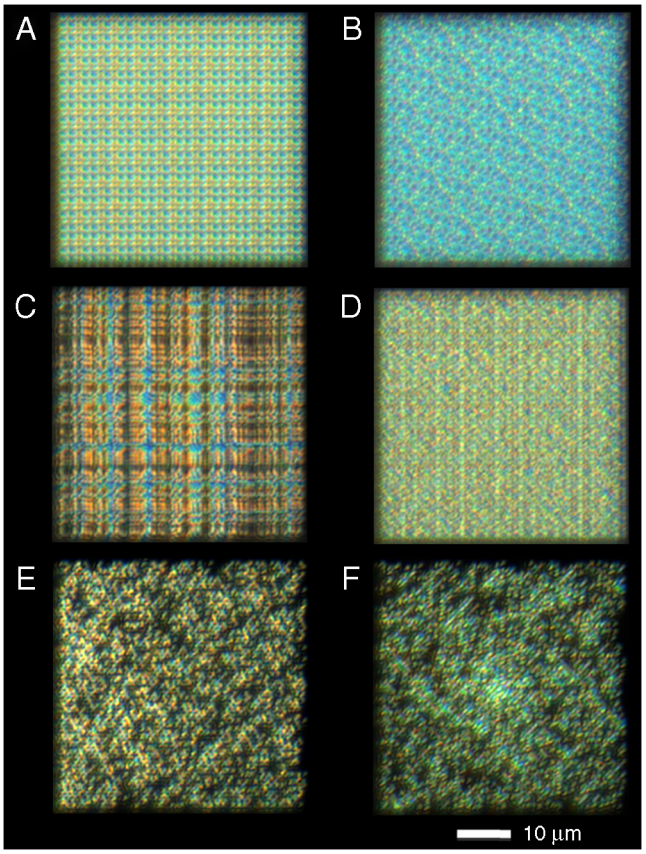

Fig. S2. Dark-field scattering images of additional colorimetric fingerprints (*A*) Fibonacci, (*B*) Penrose, (*C*) Galois, (*D*) CoPrime, (*E*) Prime and (*F*) Ulam-Spiral aperiodic arrays of 100-radius and 40 nm-high cylindrical Cr nanoparticles on a quartz substrate.

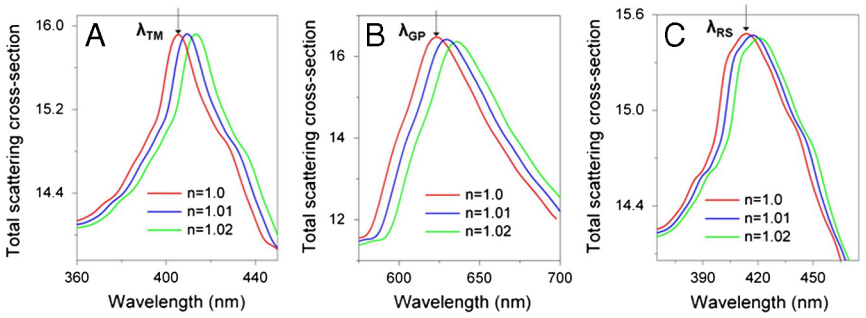

Fig. S3. Calculated red-shifts of the peaks in the total scattering efficiency of (*A*) Thue-Morse, (*B*) Gaussian prime, and (*C*) Rudin-Shapiro aperiodic arrays of 200 nm-diameter Cr nanoparticles with the change of the ambient refractive index from $n = 1.0$ (red) to $n = 1.01$ (blue) to $n = 1.02$ (green). The nearest center-to-center interparticle separation is 300 nm for the Gaussian prime array and 400 nm for Thue-Morse and Rudin-Shapiro arrays. The arrows indicate the wavelengths of the resonant peaks in the scattering spectra of the arrays in air.

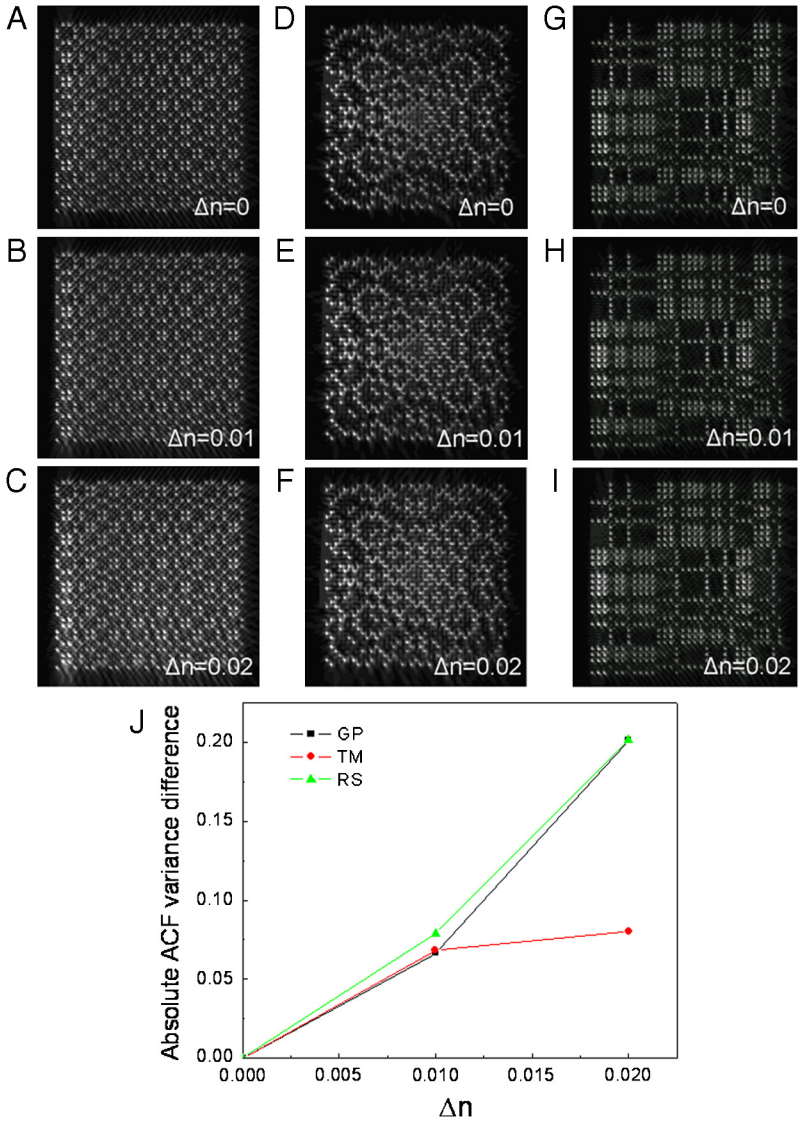

Fig. S4. In-plane field intensity distributions in the Thue-Morse (*A–C*), Gaussian prime (*D–F*), and Rudin-Shapiro (*G–I*) arrays calculated at the corresponding resonant peak wavelengths for $\Delta n = 0$ (indicated by arrows in Fig. S3): (*A–C*): $\lambda_{TM} = 405.2$ nm (*D–F*): $\lambda_{gp} = 623.15$ nm, (*G–I*): $\lambda_{RS} = 413.7$ nm. (*J*) The change of the variances of the ACF of the calculated intensity distributions with the increase of the ambient refractive index.